

# Early Paleozoic basement diorite of arc-magmatism from Kutch basin, Western India

Piyush Gupta<sup>1,2</sup> · Sandeep Singh<sup>2</sup> · Shakti Singh Rathore<sup>1</sup> · Argha Narayan Sarkar<sup>2</sup>

Received: 22 August 2023 / Revised: 17 October 2023 / Accepted: 2 November 2023 / Published online: 15 November 2023  
© The Author(s), under exclusive licence to Science Press and Institute of Geochemistry, CAS and Springer-Verlag GmbH Germany, part of Springer Nature 2023

**Abstract** In this study, we report for the first time an Early Palaeozoic basement diorite from the drilled well Nirona-A in the Banni Half-Graben of the Kutch basin, western India. The  $^{40}\text{Ar}$ – $^{39}\text{Ar}$  dates provided a plateau age of  $441.84 \pm 2.66$  Ma and another pseudo plateau of  $441.28 \pm 5.82$  to  $388.08 \pm 16.65$  Ma for the basement diorite. These ages constrain the basement formation age to the Late Ordovician-Early Silurian period. The obtained basement ages are correlatable with the later part of Cambro-Ordovician alkaline magmatism that has been reported from the Huqf area in Central Oman, whereas their lithological and petrographic correlativity with basement diorites occurring in the Dinsi Body of Nagar Parkar igneous complex in Pakistan can also be envisaged. The geochemical studies characterized the diorite with enrichment of LILE (Rb, Ba, and K) and LREE (La, Ce, Nd), strong depletion of HFSE (Nb, Sr, P, and Ti), along with weakly negative Eu anomalies. The geochemical signatures indicate their petrogenetic affiliation with mantle-derived magmas, as well as their tectonic setting to be arc-related, having post-collisional continental-arc type affinity. The  $\sim 440$  Ma basement of Kutch, therefore, appears to represent the later thermal event associated with the reworked

Neoproterozoic subduction-related suite from Greater India's northwest edge, which has implications for Gondwana assembly in the northwest Indian subcontinent.

**Keywords** Kutch basin ·  $^{40}\text{Ar}$ – $^{39}\text{Ar}$  ages · Early palaeozoic basement · Continental-arc magmatism · Calc-alkaline magmatism

## 1 Introduction and geological setting

The Kutch basin is located at the southern edge of the Indus shelf, at right angles to the southern Indus fossil rift, on the western continental margin of India (Zaigham and Mallick 2000; Biswas 2005). The basin was initially formed during the Late Triassic period and is bounded to the north by the Nagar Parkar ridge, to the east by the Radhanpura-Barmer arch, and to the south by the Kathiawar uplift (Biswas 1980, 1987, 2005) (Fig. 1). The Kutch rift basin area is composed of relatively thick Quaternary and Mesozoic sediments (Biswas 1987; Singh et al. 1997; Gupta et al. 2001) with an E–W trend (Biswas 1987). The average sediment thickness in the southern coastal region is around 6 km, while it drops to 2 km beneath northern Kutch (Gupta et al. 2001; Reddy et al. 2001). The evolution of the basin was related to the rifting of both the Indian and African plates in the Late Triassic to Early Jurassic; rifting was initiated along the Delhi Trend (east to west), with resulting subsidence of the block between the Nagar Parker fault in the north and the North Kathiawar fault in the south (Biswas 1980, 1987). However, the existence of the Kutch rift system has been questioned in some recent studies (e.g., Siawal et al. 2019), which support the continuity of the Kutch basin with the South Indus shelf, with Saurashtra

**Publisher's Note** Springer Nature remains neutral with regard to jurisdictional claims in published maps and institutional affiliations.

✉ Sandeep Singh  
sandeep.singh@es.iitr.ac.in; san662005@gmail.com

<sup>1</sup> Geochronology Laboratory, KDMIPE, Oil and Natural Gas Corporation Ltd., 9, Kaulagarh Road, Dehradun 248195, India

<sup>2</sup> Department of Earth Sciences, Indian Institute of Technology, Roorkee 247667, India

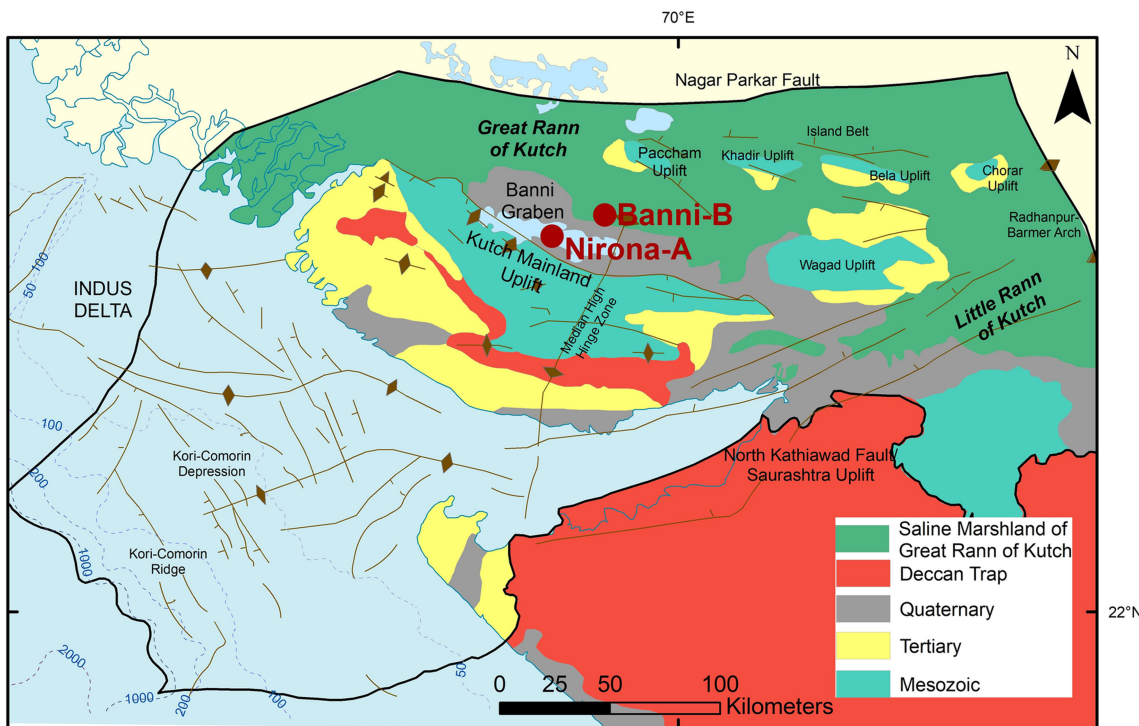


**Fig. 1** Geological map of Kutch basin showing the location of studied well Nirona-A (after Biswas 2005)

being the eastern margin of the basin, thus proposing their basements to be continuous.

The Kutch basin slopes toward WSW and is characterized by numerous Late Cretaceous uplifts with associated plutonic bodies and intervening Tertiary basins. (Biswas 1987) (Fig. 1). The Deccan traps in the basin are restricted toward the southern part of the Kutch mainland between Lakhpat in the west and Anjar in the east. The Kutch Onland Basin contains four subparallel ridges or positive topographic elements: Nagar Parkar–Tharad, the Island Belt, Wagad, and the Kutch Mainland, as well as five principal faults: the Nagar Parkar fault, the Island Belt fault, the South Wagad fault, the Kutch Mainland fault, and the North Kathiawar fault (Biswas 1987; Mathew et al. 2006) (Fig. 1).

Several Mesozoic sequence inliers appear as ‘islands’ in the eastern Rann of Kutch: Patcham, Bela, Kadir in the north, and Wagad along its axial portion, followed by a narrow-complicated basin. This half-graben sub-basin is deepened due west by a significant eastward fault in the north and the Kutch Mainland fault. Karanth and Gadhwani (2007) referred to the Kutch Mainland fault as the ‘Banni Footwall Syncline’ or the ‘Banni Half Graben’. The Mesozoic series, which includes the coarse clastics, limestone, marlstone, and shales, lie on the Precambrian bedrock in the Banni Half Graben, followed by the Tertiary sequence. A notable aspect of this block is the absence of

the Deccan Trap in the subsurface (well data) or in exposure and contains the oldest known Mesozoics. The basement has been discovered in two drilled wells, Banni-B and Nirona-A, located on the northern and southern edges of the Banni Half Graben, respectively. The lithology of the subsurface core recovered from well Banni-B is granitic-porphphyry, aplite, and rhyolitic, whereas the lithology of the subsurface core obtained from well Nirona-A is dioritic.

In this paper, we present the first report of a Cambro-Ordovician basement diorite encountered in the drilled basement of well Nirona-A in the Banni Half-Graben of the Kutch basin, based on  $^{40}\text{Ar}$ - $^{39}\text{Ar}$  dating and geochemical characterization of the recovered basement core. New data reported in this paper also provide evidence of continental arc-type magmatism in the studied basement, which may have geochronological and petrogenetic constraints and implications for Gondwana assembly for the northwestern Indian subcontinent.

## 2 Sample details

The sample under consideration is part of the basement core from 2223 to 2224.45 m intervals of Nirona-A well of the Banni Half-Graben of Kutch Basin, western India. Megascopically, the diorite sample is equigranular, medium to coarse-grained with reddish brown to greyish. The thin section study shows phaneritic texture with

equigranular fine-grained groundmass and subhedral to anhedral individual grains. They are composed of about 60% plagioclase and ~40% hornblende with minor biotite, pyroxene, chlorite, epidote, and quartz (Fig. 2).

### 3 Analytical methods

For major, trace, and rare-earth elemental analysis, three samples were used because of the limited availability of the core sample, out of which one sample was analyzed for REE composition. About 25 mg of these samples were digested using a mixture of acids (3 mL HNO<sub>3</sub> and 2 mL HF) in steel Parr digestion bombs. The bomb was subjected to heating to 200 °C for roughly 24 h in the oven. The digested sample was then dried, and the residue was dissolved in 3 mL 6 N HCl and having been dried again. The final solution was made to 100 mL with 10% HNO<sub>3</sub>. The major oxide and trace element analysis was carried out on ICP-OES and ICP-MS, respectively, in the Hydro-geochemistry Lab., Geochemistry Group of KDMIPE, Dehradun. Geological standards BCR-2 and BHVO-2 were used for calibrating the instrument.

For <sup>40</sup>Ar–<sup>39</sup>Ar analysis, fresh chips of the core samples were selected, crushed and cleaned with MilliQ water and sieved to 60–80 mesh size. Approximately, 40 mg of samples were packed in ~0.8 mm quartz vials, sealed in 0.2 mm thick cadmium cylinder, and irradiated in the core of the Dhruva Reactor at Bhabha Atomic Research Centre (BARC). The conversion of <sup>39</sup>K to <sup>39</sup>Ar by neutron irradiation was monitored with MMHb-1 (Minnesota hornblende reference material having reported age of

523 ± 2.6 Ma; Renne et al. 1998). For estimation of neutron fluence variation in samples and standards, high-purity nickel wires were irradiated along with the samples.

The isotopic composition of irradiated samples were measured in a Thermo Fisher ARGUS-VI mass spectrometer in which Ar released was extracted in typically 14 heating steps with incremental heating up to 1450 °C. One set of blank measurements corresponding to each sample heating step was carried out before the sample analysis for blank correction. The <sup>40</sup>Ar blank has been typically 1%–2% or less for all the temperature steps. The neutron fluence variation caused at the time of irradiation was calculated using <sup>58</sup>Co Gamma-activity of the irradiated nickel wires on an HPGe Coaxial Well Detector (ORTEC-GWL series) at UGC-DAE-CSIR center in Kolkata. The raw data for all samples were reduced using the ArArCALC software of Koppers (2002). The plateau age estimates contain a minimum of 50% of the total <sup>39</sup>Ar released along with four or more successive degassing steps where the mean ages overlap at the 2σ level excluding the error contribution (0.5%) from the J value.

## 4 Results

### 4.1 Major and trace element characteristics

The three studied core samples are characterized by low to moderate (51.75–52.98 wt%) SiO<sub>2</sub>. A/CNK and A/NK ratios [A/CNK = molar Al<sub>2</sub>O<sub>3</sub>/(CaO + Na<sub>2</sub>O + K<sub>2</sub>O); A/NK = molar Al<sub>2</sub>O<sub>3</sub>/(Na<sub>2</sub>O + K<sub>2</sub>O)] range from 0.76 to 0.87 and 1.50 to 1.68, respectively, suggesting metaluminous nature, with Al<sub>2</sub>O<sub>3</sub> contents varying from 16.89 to

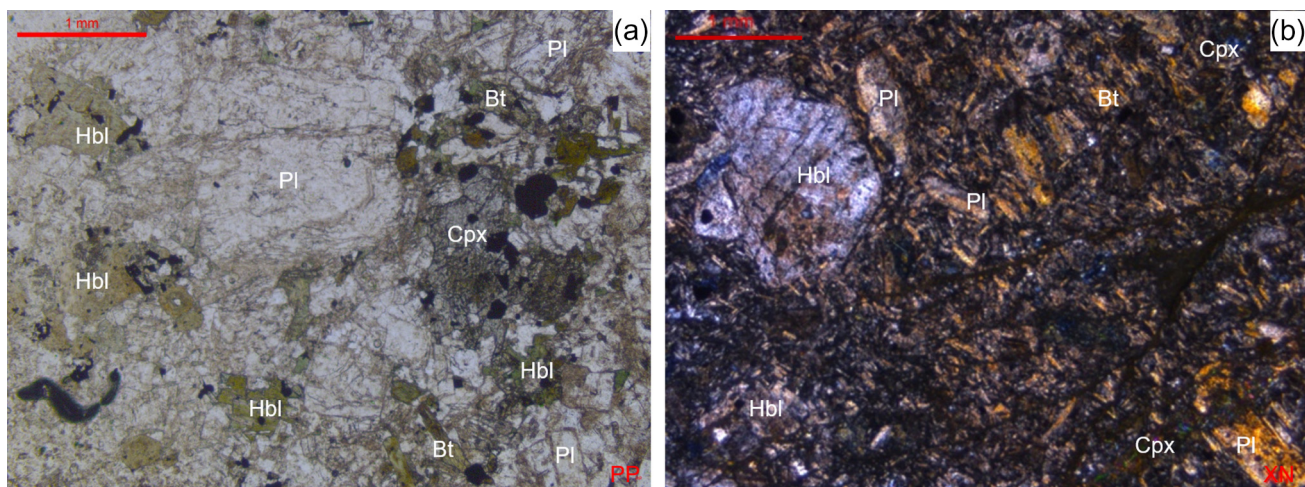


**Fig. 2** Photomicrographs of basement core samples from well Nirona-A **a** medium to coarse-grained diorite dominated by stubby plagioclase laths showing both Carlsbad and polysynthetic twinning, with subhedral pleochroic biotite forming aggregates together with green subhedral hornblende. Minor pyroxene and quartz are also observed. **b** Porphyroclasts of plagioclase laths and hornblende are surrounded by a finer matrix of biotite, chlorite, and quartz. Standard abbreviations for labelling have been adopted from Kretz (1983)

19.04 wt%, K<sub>2</sub>O ranging from 1.81 to 2.41 wt%, Na<sub>2</sub>O varying from 5.24 to 5.69 wt%, and CaO varying between 5.85 and 6.51 wt% (Table 1). The Mg# [Mg# = molecular Mg# = 100 × Molar Mg<sup>2+</sup>/(Mg<sup>2+</sup> + total Fe<sup>2+</sup>)] ranges from 46.2 to 48.8 (Table 1). The studied rocks plotted in the field of monzo-diorite, on the SiO<sub>2</sub> versus total alkali diagram (Fig. 3a; Middlemost 1994). The K<sub>2</sub>O versus SiO<sub>2</sub> plot of Rickwood (1989), further shows the samples to be of high-K calc-alkaline affinity (Fig. 3b).

The chondrite-normalized rare-earth element (REE) pattern (Fig. 4a) of the available dataset indicates that the dioritic sample is enriched with strong fractionation of LREE over HREE (LREE/HREE ratio = 14.9) with negative Eu anomaly (Eu/Eu\* = 0.83), and (La/Sm)<sub>N</sub> = 3.03–3.78 for all samples. In the primitive mantle-normalized spider diagram (Fig. 4b), samples display a negative slope, with an average (Ba/Yb)<sub>N</sub> of 22.58. The diagram also indicates strong enrichment of large ion lithophile (LILE) elements, such as Ba, K, and Rb, and LREE, including La and Ce, relative to the primitive mantle, and significantly negative anomaly of Nb, with negative anomalies of Sr (except for sample 2551), P and Ti, relative to the neighboring elements.

#### 4.2 <sup>40</sup>Ar–<sup>39</sup>Ar geochronology

Two samples from drilled well Nirona-A were analyzed for <sup>40</sup>Ar–<sup>39</sup>Ar dating and stepwise analytical data are given in Table 2, out of which sample no. 2551 was able to yield a meaningful <sup>40</sup>Ar–<sup>39</sup>Ar plateau age (Fig. 5a), whereas sample no. 2550 yielded a pseudo plateau with 6 noncongruent steps (Fig. 5b).

The sample No. 2551 yielded a 4-step plateau constituting 60.79% of the <sup>39</sup>Ar release and age of 441.84 ± 2.66 Ma (2σ) (Fig. 5a). The normal and reverse isochrons provided ages of 452.27 ± 13.83 and 452.34 ± 14.38 Ma with total fusion age of 422.58 ± 0.84 Ma (2σ) (Table 2). However, sample no. 2550 defines a pseudo plateau of 6 near-congruent steps constituting a total of 57.5% of the <sup>39</sup>Ar release, and defines two relatively flat portions, without meeting the requirements for a plateau age, and for which average ages have been calculated: 388.08 ± 16.65 and 441.28 ± 5.82 Ma, with 39.13% and 18.38% of <sup>39</sup>Ar release, respectively (Fig. 5b). The total integrated age for the above two pseudo plateaus is calculated to be 403.78 ± 23.67 Ma (2σ) (Fig. 5b). However, the pseudo plateau age yielded at higher temperature steps (441.28 ± 5.82 Ma) would in this case represent the closest age to the emplacement of the studied sample, and it is also similar to the plateau age obtained from sample no. 2551.

**Table 1** Major and Trace element compositions of the diorites in the well Nirona-A from Kutch basin

Sample	2550	2551	2550-1
SiO <sub>2</sub>	52.98	51.75	52.6
TiO <sub>2</sub>	1.87	1.85	1.92
Al <sub>2</sub> O <sub>3</sub>	19.04	18.9	16.89
FeO <sub>(T)</sub>	7.46	7.57	7.75
MnO	0.15	0.14	0.11
MgO	3.60	4.05	3.92
CaO	5.85	6.51	6.02
Na <sub>2</sub> O	5.69	5.24	5.35
K <sub>2</sub> O	1.81	2.41	2.25
P <sub>2</sub> O <sub>5</sub>	0.55	0.57	0.61
LOI	0.89	0.72	2.08
Total	99.89	99.71	99.50
A/CNK	0.87	0.82	0.76
A/NK	1.68	1.68	1.50
Mg#	46.24	48.81	47.41
<i>CIPW norms</i>			
Q			
Or	10.7	14.24	13.3
Ab	43.72	34.92	41.01
An	21.06	20.93	15.43
C			
Di	3.62	6.30	8.63
Hy			
Ol	11	10.96	9.96
Mt	1.80	1.83	1.87
Il	3.55	3.51	3.65
Ap	1.27	1.31	1.41
Ne	2.40	5.10	2.31
<i>Trace elements (ppm)</i>			
Rb	40.39	65.59	27.43
Ba	531.63	1169	298.35
Th	8.64	8.52	4.58
Nb			1.40
Sr	642.98	1056	301.44
V	248.90	256.9	89.51
Zr	164.57	164.07	169.72
Y	24.48	24.08	19.37
<i>Rare earth elements (ppm)</i>			
La	30.17	30.95	30.31
Ce	75.04	76.78	63.75
Pr			6.82
Nd	40.08	41.2	27.04
Sm	6.18	6.37	5.01
Eu			1.25
Gd			4.10
Tb			0.537
Dy			2.738
Ho			0.519

**Table 1** continued

Sample	2550	2551	2550-1
Er			1.483
Tm			0.197
Yb	2.39	2.33	1.263
Lu			0.189

## 5 Discussion

### 5.1 Temporal and spatial evolution constraints

Since the occurrence of basement outcrops in the Kutch basin is extremely rare as a result of a large sediment thickness, the lithological and petrogenetic variation in different basement types throughout and across the basin is not yet fully understood. Except for a few drill holes e.g., Banni and Nirona regions, the opportunity to recover and analyze basement samples has been limited.

The closest instance of basement rocks in outcrop in the Kutch area has been encountered in the Nagar Parkar igneous complex in Pakistan. Bordering the northern flank of the graben, it forms an uplifted block where basement rocks are only intermittently exposed and physio-graphically undetectable (Kazmi and Khan 1973). The lithology of the Nagar Parkar complex ranges from riebeckite-aegirine granite to biotite hornblende granite, acid dykes, rhyolite plugs, and basic dykes (Jan et al. 1997), and their Late Proterozoic ages span from 1000 to 1100 Ma (Karunjhar grey granite) to 700–800 Ma (pink and other

granites) (Khan et al. 2012). In the Nagar Parkar igneous complex, Jan et al. (2014) described an individual body of the basement which they named ‘Dinsi body’, that displays a dioritic basement ranging from varieties having large amounts of hornblende to those with essential quartz, and occurs with granite, dolerite, and rare rhyolite patches and dykes.

Being the first report of a dioritic basement encountered in the Kutch basin, it is difficult to correlate this basement type with a reported occurrence of similar petrological characters from close vicinity. However, petrographically, the studied basement can be correlated with the reported basement in the Dinsi body, as substantial diorite-type basements have not been reported in the northwestern part of the Indian subcontinent so far.

Furthermore, intrusions of Cambro-Ordovician alkaline magmatism have been reported from the Huqf area of Central Oman (Worthing 2005; Worthing and Nasir 2008), where the presence of two pulses of magmatism at 513–526 Ma and 452–462 Ma was suggested by Worthing and Nasir (2008) based on  $^{40}\text{Ar}$ – $^{39}\text{Ar}$  geochronology. The intrusion of these magmatic rocks may have been sourced from enriched protolith by supra-subduction zone fluids (Worthing and Nasir 2008) and formed due to tectonic and structural events associated with the second cycle of intracratonic rifting influenced by the widespread Najd extensional event in the Oman basin (Ries and Shackleton 1990; Loosveld et al. 1996; Worthing and Nasir 2008). Geochronologically, the ages obtained in the present analysis can be correlated with the later event of

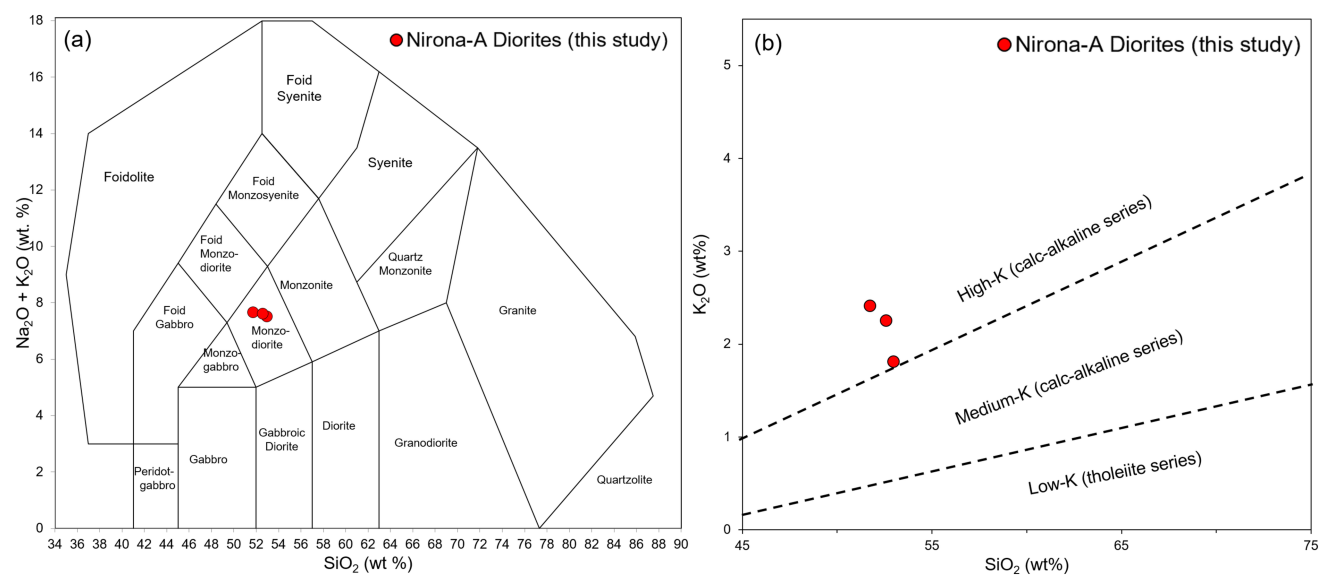
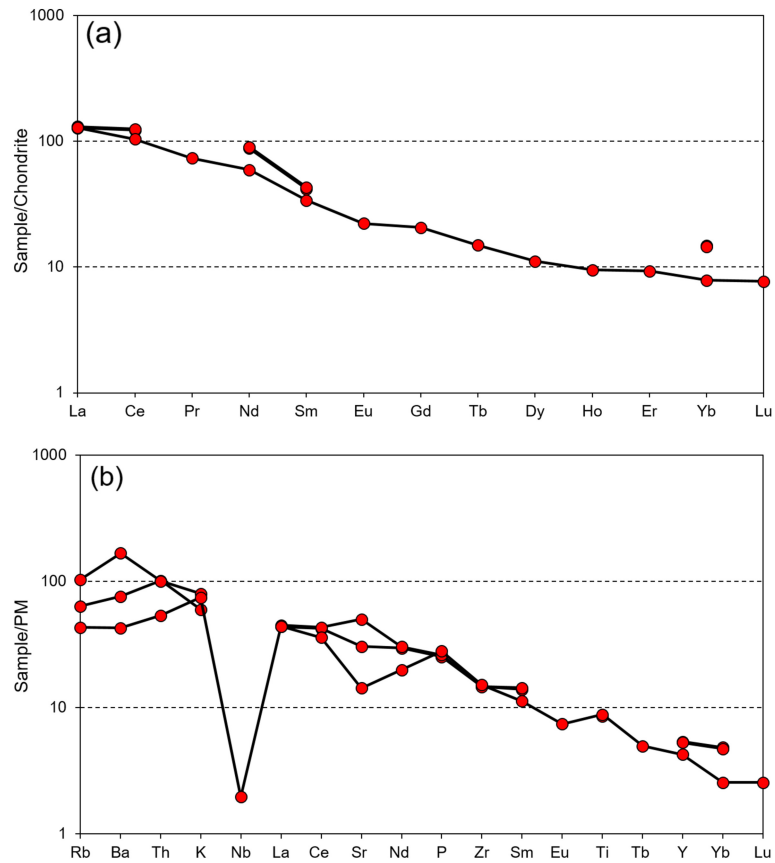


**Fig. 3** **a** Major element classification diagrams illustrating the Nirona-A diorites on a total alkali versus silica diagram (Middlemost 1994) **b** Subdivision of sub-alkaline rocks using K<sub>2</sub>O versus SiO<sub>2</sub> diagram for studied diorite samples (after Rickwood 1989)

**Fig. 4** **a** Chondrite-normalized REE patterns and **b** primitive mantle-normalized trace element spider diagrams for studied samples from well Nirona-A, Kutch basin. Chondrite and primitive mantle values from Sun and McDonough (1989)



magmatism reported from the Huqf area, Central Oman, as a part of the widespread extensional event in the Najd rift system.

## 5.2 Petrogenesis and tectonic setting

Petrogenetically, the generation of dioritic magmas can be attributed to either partial melting of crustal components or fractional crystallization of mantle-derived mafic magmas (McDermott et al. 1996; Liu et al. 2008). In general, for the generation of intermediate rocks such as diorites, the most accepted models include (1) partial melting of herzburgite in the mantle wedge, modified by H<sub>2</sub>O-rich fluids or melts released from a subducting slab (e.g., Carmichael 2002); (2) fractional crystallization of mantle-derived basaltic magma in shallow or deep crustal magma chambers (e.g., Grove et al. 2003; Annen et al. 2006); or (3) magma mixing between silicic magmas of crustal origin and mantle derived mafic magmas (e.g. Annen et al. 2006). Diorites produced in the mantle wedge or by differentiation of mantle-derived magmas tend to exhibit higher MgO contents with high Mg# (Grove et al. 2003), which is usually Mg# >40 in case of melts characterized by involvement of a mantle component as compared to Mg# <40 for those derived from crustal derived melts (Rapp and Watson

1995). In addition, Rb/Sr ratios also provide a useful index to distinguish between crustal and mantle sources (e.g., 0.32–0.95 for crustal origin and 0.01–0.1 for mantle-derived rocks; Taylor and McLennan 1985).

The diorites in the present study are characterized by higher MgO (3.6–4.05) and Mg# values (46.2–48.8), and low Rb/Sr ratios (0.06–0.09), revealing the role of mantle-derived melts in the generation of these rocks. This is further demonstrated in the SiO<sub>2</sub> versus Mg# plot (Fig. 6a), where all the samples lie close to the field of mantle-derived melts.

Certain major oxides such as TiO<sub>2</sub>, Al<sub>2</sub>O<sub>3</sub>, P<sub>2</sub>O<sub>5</sub>, etc., and whole-rock trace elements like Ce, Zr, and Y along with ratios like La/Yb and Th/Yb have been identified in studies as significant contributors to constrain different tectonic settings (Müller et al. 1992; Müller and Groves 1995; Condé 1989). The studied basement diorites, being high-K calc-alkaline rocks (Fig. 3b), can occur in various geotectonic settings, such as continental, oceanic, post-collisional, and within the plate (Müller et al. 1992). In order to delineate the samples for their arc-related versus within-plate affiliation, the discrimination diagrams based on major oxides, Al<sub>2</sub>O<sub>3</sub> versus TiO<sub>2</sub> and HFSEs, Zr versus Y plot (Fig. 6b&c; Müller et al. 1992), respectively, were used, which shows that the diorite samples in study appear

**Table 2**  $^{40}\text{Ar}$ – $^{39}\text{Ar}$  Analytical data for studied samples

Incremental heating step	$^{36}\text{Ar}_{(\text{a})}$ [fA]	$^{37}\text{Ar}_{(\text{ca.})}$ [fA]	$^{38}\text{Ar}_{(\text{cl})}$ [fA]	$^{39}\text{Ar}_{(\text{k})}$ [fA]	$^{40}\text{Ar}_{(\text{r})}$ [fA]	Age $\pm 2\sigma$ (Ma)	$^{40}\text{Ar}_{(\text{r})}$ (%)	$^{39}\text{Ar}_{(\text{k})}$ (%)	K/Ca $\pm 2\sigma$
<i>Sample No. 2551</i>									
350 °C	7.64	18.43	9.77	16.26	6327.46	228.00 $\pm$ 2.09	73.70	3.03	0.379 $\pm$ 0.075
550 °C	0.84	10.95	1.27	2.62	960.70	215.38 $\pm$ 6.28	79.34	0.49	0.103 $\pm$ 0.013
620 °C	2.74	32.05	4.51	16.58	7578.88	265.11 $\pm$ 1.99	90.32	3.08	0.222 $\pm$ 0.012
680 °C	3.83	72.86	7.84	33.65	12688.27	221.38 $\pm$ 0.83	91.79	6.26	0.199 $\pm$ 0.006
740 °C	3.40	30.44	6.75	25.35	18448.51	405.49 $\pm$ 1.17	94.83	4.72	0.358 $\pm$ 0.021
850 °C	5.58	32.53	12.21	48.93	38614.58	435.92 $\pm$ 1.46	95.90	9.10	0.647 $\pm$ 0.031
940 °C	7.82	180.69	23.04	91.72	73690.68	442.92 $\pm$ 0.90	96.96	17.06	0.218 $\pm$ 0.003
1000 °C	6.46	125.63	26.08	91.39	73142.23	441.38 $\pm$ 0.87	97.45	17.00	0.313 $\pm$ 0.006
1080 °C	7.24	105.43	33.27	94.77	76226.26	443.33 $\pm$ 0.85	97.26	17.63	0.387 $\pm$ 0.009
1150 °C	10.06	162.08	46.95	78.18	67300.74	470.73 $\pm$ 1.03	95.77	14.54	0.207 $\pm$ 0.004
1200 °C	6.74	59.34	26.53	27.78	25923.14	505.17 $\pm$ 1.24	92.86	5.17	0.201 $\pm$ 0.006
1450 °C	7.09	32.89	10.77	10.31	8773.29	466.00 $\pm$ 3.83	80.70	1.92	0.135 $\pm$ 0.007
<i>Sample No. 2550</i>									
450 °C	6.40	19.31	2.94	4.66	289.14	37.68 $\pm$ 4.09	13.25	1.14	0.104 $\pm$ 0.017
500 °C	11.86	58.05	5.64	12.71	660.47	31.64 $\pm$ 2.64	15.85	3.10	0.094 $\pm$ 0.004
550 °C	11.31	95.87	8.23	19.91	1824.87	55.43 $\pm$ 1.73	35.30	4.86	0.089 $\pm$ 0.002
620 °C	9.89	154.52	12.00	33.08	4443.43	80.67 $\pm$ 2.16	60.30	8.07	0.092 $\pm$ 0.002
740 °C	10.61	286.60	21.44	55.90	12390.28	131.27 $\pm$ 0.61	79.79	13.64	0.084 $\pm$ 0.001
850 °C	11.82	122.07	18.73	47.89	25053.05	295.75 $\pm$ 1.59	87.75	11.68	0.169 $\pm$ 0.004
940 °C	8.90	177.85	14.54	51.68	34896.48	373.43 $\pm$ 0.92	92.98	12.61	0.125 $\pm$ 0.002
1000 °C	3.95	204.49	12.74	39.61	28788.18	399.03 $\pm$ 0.95	96.09	9.66	0.083 $\pm$ 0.001
1080 °C	6.50	168.54	27.18	69.14	49503.10	393.70 $\pm$ 1.00	96.26	16.86	0.176 $\pm$ 0.003
1150 °C	8.22	303.64	34.92	42.83	34722.00	439.87 $\pm$ 1.03	93.45	10.45	0.061 $\pm$ 0.001
1200 °C	4.49	98.36	22.67	19.19	15629.52	441.64 $\pm$ 1.68	92.16	4.68	0.084 $\pm$ 0.003
1450 °C	5.89	88.26	16.88	13.34	11115.07	450.63 $\pm$ 2.76	86.45	3.25	0.065 $\pm$ 0.002

to be of arc-related affinity, as all of the samples cluster in the arc-related field.

Further, since the analysed samples are of high-K calc-alkaline affinity (Fig. 3b), and are characterized by an enrichment in LILE (e.g., Rb, Ba, and K) and LREE (La, Ce, Nd), with strong depletion in HFSE (Nb, Ta, Sr, P, and Ti) (Fig. 4). The affinities of these samples, therefore, appear to be of calc-alkaline magmatism in active continental margins generated in a subduction-related (continental-arc or oceanic-arc) setting (e.g., Qi et al. 2014, and references therein).

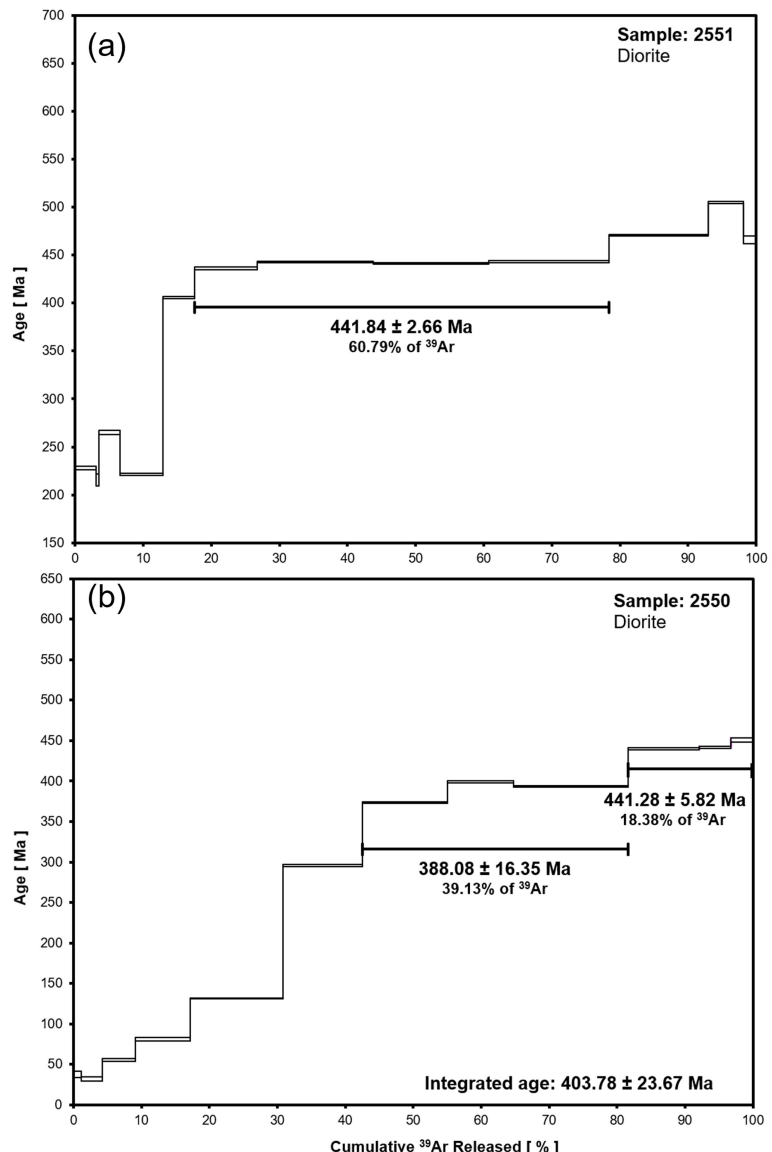
In order to demarcate whether the studied samples belong to continental- or oceanic-arc setting, tectonic setting discrimination diagram of Müller et al. (1992) was utilized (Fig. 6d), in which the studied high-K calc-alkaline diorites are plotted in the continental-arc field in  $\text{TiO}_2/\text{Al}_2\text{O}_3$  versus  $\text{Zr}/\text{Al}_2\text{O}_3$  plot (Fig. 6d). This is also evident in the  $\text{La/Yb}$  versus  $\text{Th/Yb}$  tectonic discrimination diagram

(Fig. 6e; Condie 1989) which suggests the tectonic setting to be of the continental margin arc affinity. The depletion of Nb and Ti relative to LILE and LREE and the low Nb/La ratio observed in the studied samples (Fig. 4) are further distinctive features of convergent plate margin magmatism (e.g., Hawkesworth et al. 1991; Castillo et al. 2007). Further building on the interpretation, the  $\text{Zr}/\text{TiO}_2$  versus  $\text{Ce}/\text{P}_2\text{O}_5$  plot (Fig. 6f; Müller et al. 1992) concludes that the samples show post-collisional continental-arc type setting in terms of their geotectonic environment.

### 5.3 Implications to Gondwana assembly

The north-western margin of Greater India has several extensive subduction-related mid-Neoproterozoic igneous suites (e.g. Hill and Walter 2000; Tucker et al. 2001; Ashwal et al. 2002; Li et al. 2006; Piper 2007; Thomas et al. 2009; Van Lente et al. 2009; Dhama Rao et al. 2013;

**Fig. 5** Age spectra for samples from well Nirona-A, with the sample name, rock type, plateau age, and percentage of gases on which it is calculated. **a** Plateau age of sample 2551 and **b** Pseudoplateau ages of sample No. 2550



Qi et al. 2014), and protoliths of mid-Neoproterozoic ages in high-pressure metamorphic suites (e.g. North Lhasa terrane, Zang et al. 2012, 2014) reported in published literature. Notably, high-K calc-alkaline granitoid reported by Qi et al. (2014) from the northeastern margin of the Indochina block are similar in age and tectonic setting to those occurring along the northwestern margin of Greater India. Similarly, the presence of a subduction system in the northern margin of the amalgamated Gondwanaland during the Cambro–Ordovician time (Dalziel 1997; Unruh 1997, Singh and Dhiman 2021) has been suggested, which recorded a very widespread thermal event in the Greater

India that is now exposed within Higher Himalayan Crystallines and Thethyan Sedimentary sequences (Singh and Jain 2003). The probable position of Kutch basement has been shown in the paleogeographic reconstruction at mid-Neoproterozoic period depicting juxtaposition of greater Indian block in a mid-Neoproterozoic magmatic belt against an eastward subducting ocean (Fig. 7a), and at Cambro–Ordovician period showing the subduction system along northern margin of amalgamated Gondwana (Fig. 7b). However, due to the limited geochronological and geochemical data, more samples need to be recovered and analysed from the study area for their geochronology,

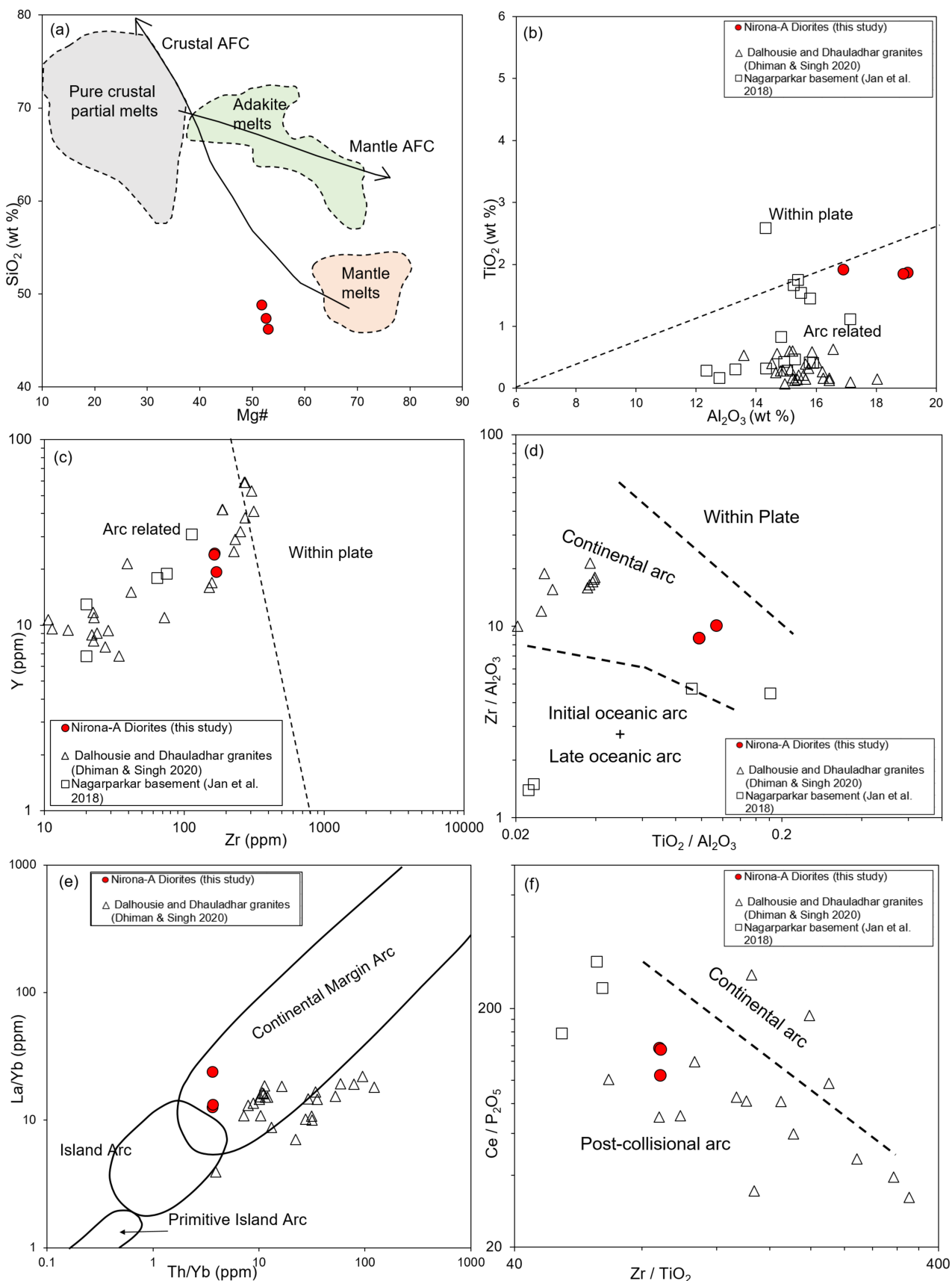


**Fig. 6** **a**  $\text{SiO}_2$  (wt%) versus Mg# diagram (the curves of mantle assimilation-fractional crystallization (AFC) and crustal AFC are after Stern and Kilian 1996; Tectonic discrimination diagrams **b**  $\text{Al}_2\text{O}_3$  (wt%) versus  $\text{TiO}_2$  (wt%) **c**  $\text{Zr}$  (ppm) versus  $\text{Y}$  (ppm) **d**  $\text{TiO}_2/\text{Al}_2\text{O}_3$  versus  $\text{Zr}/\text{Al}_2\text{O}_3$  (after Müller et al. 1992); **e**  $\text{La/Yb}$  versus  $\text{Th/Yb}$  plot (after Condie 1989); **f**  $\text{Zr}/\text{TiO}_2$  versus  $\text{Ce}/\text{P}_2\text{O}_5$  plot (after Müller et al. 1992). The hollow triangles and squares represent published data from Dalhousie and Dhauladhar granites (Dhiman and Singh 2021), and Nagar Parkar basement rocks (Jan et al. 2018), respectively, which show similar tectonic affinities as compared with the studied samples from Nirona-A.

geochemistry, and paleo-magnetism, in order to evaluate the position and tectonic relationship of the Kutch basement with Greater India and related landmasses during Late Neoproterozoic and Early Palaeozoic.

The data from coeval plutons (e.g. Dalhausie and Dhauladhar granites; Singh and Dhiman 2021) as well as other similar basement rocks in the area (e.g. Nagar Parkar igneous complex; Jan et al. 2018) also display similar geotectonic setting as compared to the studied diorite basement of Nirona-A (Fig. 6). The first-time reported  ${}^{40}\text{Ar}-{}^{39}\text{Ar}$  ages of  $\sim 440$  Ma (Fig. 5) for the dioritic basement from the Kutch basin do appear to be younger as compared to other mid-Neoproterozoic subduction-related suites reported by the above workers, however, these may reflect the later thermal event associated with Cambro-Ordovician continental-arc magmatism in Greater India by reworking of existing Neoproterozoic granites (e.g. Dhiman and Singh 2021).

## 6 Conclusions

Present geochronological and geochemical data for the basement rocks recovered from drilled hole Nirona-A from Banni Half-Graben of the Kutch onshore basin core provide new  ${}^{40}\text{Ar}-{}^{39}\text{Ar}$  age constraints of  $441.84 \pm 2.6$  Ma for the Kutch basin. Petrographically, the studied basement type can be correlated with the reported dioritic Dinsi Body in Nagar Parkar igneous complex based on their close spatial proximity, as well as their temporal continuity can be visualized with the Cambro-Ordovician alkaline magmatism reported from Huqf area in Central Oman based on similar emplacement ages.

The major, trace, and REE geochemistry of the analyzed samples have indicated towards their petrogenetic affiliation with mantle-derived magmas, as well as their tectonic setting being arc-related, having post-collisional continental-arc type affinity. However, the limited dataset available due to the scarce nature of core samples is not sufficient to conclusively establish the petrogenesis and tectonics of the studied basement, which may be firmed up by recovery and analyses of several more basement samples from the Banni Half-Graben in the Kutch basin. In all probability, the Kutch Early-Paleozoic basement may represent the later thermal event associated with reworked Neoproterozoic subduction-related suite from Greater India's northwest edge, which has implications for Gondwana assembly in the northwest Indian subcontinent.

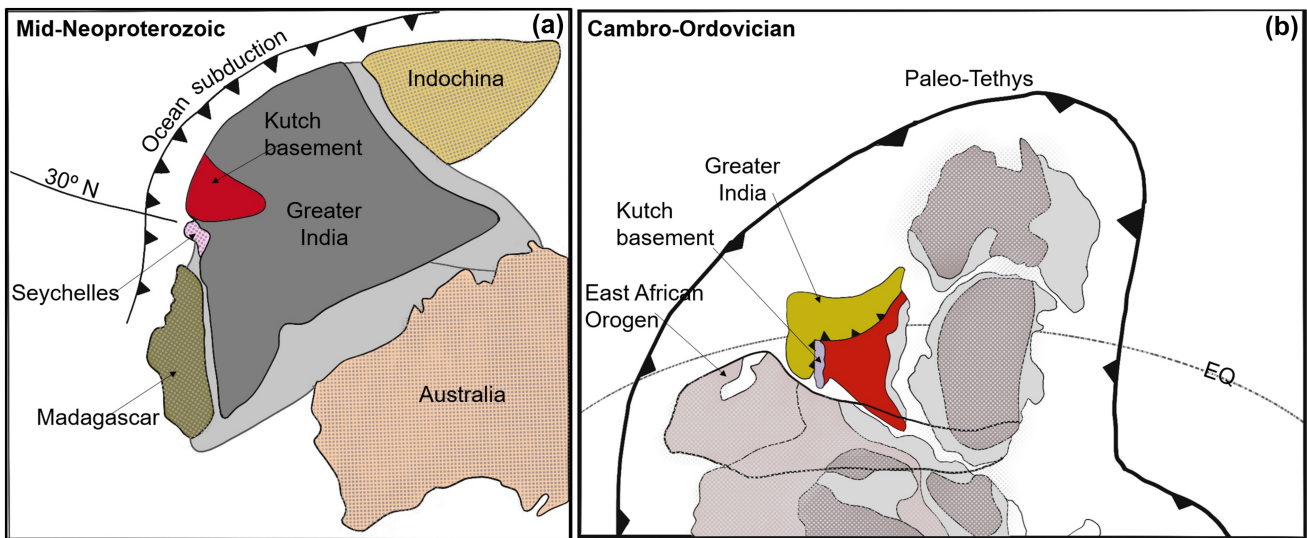


**Fig. 7** **a** Paleogeographic reconstruction depicting juxtaposition of greater Indian block (showing the probable position of Kutch basement), Seychelles, and Madagascar along with Indochina block defining a middle Neoproterozoic magmatic belt against an eastward subducting ocean (modified after Qi et al. 2014), **b** Reconstruction of Gondwanaland during Cambro-Ordovician showing the presence of the subduction system along the northern margin of amalgamated Gondwanaland (modified after Dhiman and Singh 2021)

## Declarations

**Conflict of interest** The authors declare that they have no known competing financial interests or personal relationships that could have appeared to influence the work reported in this paper.

## References

- Annen C, Blundy JD, Sparks RSJ (2006) The genesis of intermediate and silicic magmas in deep crustal hot zones. *J Petrol* 47:505–539
- Ashwal LD, Demaiffe D, Torsvik TH (2002) Petrogenesis of neoproterozoic granitoids and related rocks from the Seychelles: the case for an Andean-type arc origin. *J Petrol* 43(1):45–83
- Biswas SK (1980) Structure of Kutch-Kathiawar region, Western India. In: Proc. 3rd Indian Geological Congress, Pune, pp 255–272
- Biswas SK (1982) Rift basins in western margin of India and their hydrocarbon prospects with special reference to Kutch basin. *AAPG Bull* 66(10):1497–1513
- Biswas SK (1987) Regional tectonic framework, structure and evolution of the western marginal basins of India. *Tectonophysics* 135(4):307–327
- Biswas SK (2005) A review of structure and tectonics of Kutch basin, western India, with special reference to earthquakes. *Curr Sci* 88(10):1592–1600
- Carmichael IS (2002) The andesite aqueduct: Perspectives on the evolution of intermediate magmatism in west-central (105–99°W) Mexico. *Contrib Mineral Petrol* 143:641–663. <https://doi.org/10.1007/s00410-002-0370-9>
- Condie KC (1989) Geochemical changes in basalts and andesites across the Archean-Proterozoic boundary: identification and significance. *Lithos* 23(1–2):1–8
- Dalziel IWD (1997) Overview: Neoproterozoic-Paleozoic geography and tectonics: review, hypothesis, environment speculation. *Geol Soc Am Bull* 109(1):16–42
- Dharma Rao CV, Santosh M, Kim SW, Li S (2013) Arc magmatism in the Delhi fold belt: SHRIMP U–Pb zircon ages of granitoids and implications for Neoproterozoic convergent margin tectonics in NW India. *J Asian Earth Sci* 78:83–9
- Dhiman R, Singh S (2021) Neoproterozoic and Cambro-Ordovician magmatism: episodic growth and reworking of continental crust, Himachal Himalaya, India. *Int Geol Rev* 63(4):422–436
- Grove TL, Elkins-Tanton LT, Parman SW, Chatterjee N, Muntener O, Gaetani GA (2003) Fractional crystallization and mantle-melting controls on calc-alkaline differentiation trends. *Contrib Min Petrol* 145:515–533
- Gupta HK, Harinarayana T, Kousalya M, Mishra DC, Mohan I, Rao NP, Raju PS, Rastogi BK, Reddy PR, Sarkar D (2001) Bhuj Earthquake of 26 January, 2001. *Geol Soc India* 57(3):275–278
- Hill AC, Walter MR (2000) Mid-Neoproterozoic (~830–750 Ma) isotope stratigraphy of Australia and global correlation. *Precamb Res* 100(1–3):181–211
- Jan MQ, Laghari AM, Khan MA (1997) Petrography of Nagar Parkar igneous complex, Tharparkar, Southeast Sindh. *Geol Bull Univ Peshawar* 30:227–249
- Jan MQ, Laghari A, Agheem MH, Anjum S (2014) Geology and petrography of the Nagar Parkar igneous complex, southeastern Sindh: the Dinsi body. *J Himal Earth Sci* 47(2):1
- Jan MQ, Laghari A, Khan MA, Agheem MH, Khan T (2018) Petrology of calc-alkaline/adakitic basement hosting A-type neoproterozoic granites of the Malani igneous suite in Nagar Parkar, SE Sindh, Pakistan. *Arab J Geosci* 11:1–14
- Karanth RV, Gadhavi MS (2007) Structural intricacies: emergent thrusts and blind thrusts of Central Kachchh, western India. *Curr Sci* 93(9):1271–1280
- Kazmi AH, Khan RA (1973) The report on the geology, minerals and water resources of Nagar Parkar, Pakistan. Geol Survey Pakistan, Info Release 64:1–32
- Khan T, Murata M, Rehman HU, Zafar M, Ozawa H (2012) Nagarparker granites showing Rodinia remnants in the south-eastern part of Pakistan. *J Asian Earth Sci* 59:39–51
- Koppers AA (2002) ArArCALC—software for Ar/ Ar age calculations. *Comput Geosci* 28(5):605–619
- Kretz R (1983) Symbols for rock-forming minerals. *Amer Min* 68(1–2):277–279
- Li XH, Li ZX, Wingate MT, Chung SL, Liu Y, Lin GC, Li WX (2006) Geochemistry of the 755 Ma Mundine Well dyke swarm, northwestern Australia: part of a neoproterozoic mantle superplume beneath Rodinia? *Precamb Res* 146(1–2):1–5
- Liu S, Hu R, Gao S, Feng C, Qi Y, Wang T, Coulson IM (2008) U–Pb zircon age, geochemical and Sr–Nd–Pb–Hf isotopic constraints on age and origin of alkaline intrusions and associated mafic dikes from Sulu orogenic belt, Eastern China. *Lithos* 106:365–379
- Loosveld RJ, Bell A, Terken JJ (1996) The tectonic evolution of interior Oman. *GeoArabia* 1(1):28–51
- Mathew G, Singhvi AK, Karanth RV (2006) Luminescence chronometry and geomorphic evidence of active fold growth along the Kachchh Mainland Fault (KMF), Kachchh, India: seismotectonic implications. *Tectonophysics* 422(1–4):71–87
- McDermott F, Harris NBW, Hawkesworth CJ (1996) Geochemical constraints on crustal anatexis: A case study from the Pan-African damara granitoids of Namibia. *Contrib Mineral Petrol* 123:406–423
- Middlemost EA (1994) Naming materials in the magma/igneous rock system. *Earth-Sci Rev* 37(3–4):215–224
- Müller D, Groves DI (1995) Potassic igneous rocks and associated gold copper mineralization. Springer, Berlin, p 56
- Müller D, Rock NMS, Groves DI (1992) Geochemical discrimination between shoshonitic and potassic volcanic rocks in different tectonic settings: a pilot study. *Mineral Petrol* 46:259–289
- Piper JD (2007) The Neoproterozoic supercontinent Palaeopangaea. *Gond Res* 12(3):202–227
- Qi X, Santosh M, Zhu L, Zhao Y, Hu Z, Zhang C, Ji F (2014) Mid-Neoproterozoic arc magmatism in the northeastern margin of the Indochina block, SW China: Geochronological and petrogenetic constraints and implications for Gondwana assembly. *Precamb Res* 245:207–224
- Rapp RP, Watson EB (1995) Dehydration melting of metabasalt at 8–32 kbar: implications for continental growth and crust–mantle recycling. *J Petrol* 36:891–931
- Rathore SS, Gupta P, Sarkar AN (2020) Establishment of  $^{40}\text{Ar}$ – $^{39}\text{Ar}$  dating facility and dating of basalts from Kerala Konkan Basin. Unpub. Report, KDMIPE, ONGC, Dehra Dun
- Reddy PR, Sarkar D, Sain K, Mooney WD (2001) A report on a collaborative scientific study at USGS, Menlo Park, USA. USGS Unpub Report 1–52
- Renne PR, Swisher CC, Deino AL, Karner DB, Owens TL, DePaolo DJ (1998) Intercalibration of standards, absolute ages and uncertainties in  $^{40}\text{Ar}$ – $^{39}\text{Ar}$  dating. *Chem Geol* 145(1–2):117–152
- Rickwood PC (1989) Boundary lines within petrologic diagrams which use oxides of major and minor elements. *Lithos* 22(4):247–263
- Ries AC, Shackleton RM (1990) Structures in the Huqf-Haushi uplift, east central Oman. *Geol Soc London Sp Pub* 49(1):653–663
- Siwal A, Dash PP, Srivastava HC (2019) Evolution of West Coast of India-APlate Tectonic Approach. *Bull ONGC* 54(1):147–164

- Singh D, Alat CA, Singh RN, Gupta VP (1997) Source rock characteristics and hydrocarbon generating potential of Mesozoic sediments in Lodhika area, Saurashtra basin, Gujarat, India. In: Proceedings of second international petroleum conference exhibition. Petrotech, New Delhi, pp 205–220
- Singh S, Jain AK (2003) Himalayan granitoids. *J Virtual Expl* 11:1–20
- Stern CR, Kilian R (1996) Role of the subducted slab, mantle wedge and continental crust in the generation of adakites from the Andean Austral Volcanic Zone. *Contrib Mineral Petrol* 123:263–281
- Sun SS, McDonough WF (1989) Chemical and isotopic systematics of oceanic basalts: implications for mantle composition and processes. *Geol Soc, London, Sp Pub* 42(1):313–345
- Taylor SR, McLennan SM (1985) The continental crust: its composition and evolution. Blackwell Sci Publ, Carlton, p 312
- Thomas RJ, De Waele B, Schofield DI, Goodenough KM, Horstwood MSA, Tucker R, Bauer W, Annels AE, Howard K, Walsh G, Rabarimana M, Rafa-hatelo JM, Ralison AV, Randriamananjara T (2009) Geological evolution of the Neoproterozoic Bemarivo belt, northern Madagascar. *Precamb Res* 172:279–300
- Tucker RD, Ashwal LD, Torsvik TH (2001) U–Pb geochronology of seychelles granitoids: a neoproterozoic continental arc fragment. *Earth Planet Sci Lett* 187(1–2):27–38
- Unrug R (1997) Rodinia to gondwana: the geodynamic map of gondwana supercontinent assembly. *GSA Today* 7(1):1–6
- Van Lente B, Ashwal LD, Pandit MK, Bowring SA, Torsvik TH (2009) Neoproterozoic hydrothermally altered basaltic rocks from Rajasthan, northwest India: implications for Late Precambrian tectonic evolution of the Aravalli Craton. *Precamb Res* 170(3–4):202–222
- Worthing MA (2005) Petrology and geochronology of a Neoproterozoic dyke swarm from Marbat, South Oman. *J Afr Earth Sci* 41(3):248–265
- Worthing MA, Nasir S (2008) Cambro-Ordovician potassic (alkaline) magmatism in central Oman: petrological and geochemical constraints on petrogenesis. *Lithos* 106(1–2):25–38
- Zaigham NA, Mallick KA (2000) Prospect of hydrocarbon associated with fossil-rift structures of the southern Indus basin, Pakistan. *AAPG Bull* 84(11):1833–1848
- Zhang Z, Dong X, Liu F, Lin Y, Yan R, He Z, Santosh M (2012) The making of Gondwana: discovery of 650 Ma HP granulites from the North Lhasa, Tibet. *Precamb Res* 212:107–116
- Zhang ZM, Dong X, Santosh M, Zhao GC (2014) Metamorphism and tectonic evolution of the Lhasa terrane, central Tibet. *Gond Res* 25(1):170–189

**Publisher's Note** Springer Nature remains neutral with regard to jurisdictional claims in published maps and institutional affiliations.

Springer Nature or its licensor (e.g. a society or other partner) holds exclusive rights to this article under a publishing agreement with the author(s) or other rightsholder(s); author self-archiving of the accepted manuscript version of this article is solely governed by the terms of such publishing agreement and applicable law.